Biochemical and Biophysical Research Communications 400 (2010) 94–99

Contents lists available at ScienceDirect

Biochemical and Biophysical Research Communications

journal homepage: www.elsevier.com/locate/ybbrc

The universal mechanism for iron translocation to the ferroxidase site in ferritin, which is mediated by the well conserved transit site

Taro Masuda [a,*], Fumiyuki Goto [b], Toshihiro Yoshihara [b], Bunzo Mikami [c]

[a] Laboratory of Food Quality Design and Development, Division of Agronomy and Horticultural Science, Graduate School of Agriculture, Kyoto University, Gokasho, Uji, Kyoto 611-0011, Japan
[b] Biotechnology Sector, Environmental Science Research Laboratory, Central Research Institute of Electric Power Industry, 1646 Abiko, Abiko, Chiba 270-1194, Japan
[c] Laboratory of Applied Structural Biology, Division of Applied Life Sciences, Graduate School of Agriculture, Kyoto University, Gokasho, Uji, Kyoto 611-0011, Japan

ARTICLE INFO

Article history:
Received 3 August 2010
Available online 10 August 2010

Keywords:
Ferritin
Ferroxidase site
Metal sequestration
Transit site

ABSTRACT

Ferritins are ubiquitous iron storage proteins. Recently, we identified a novel metal-binding site, transit site, in the crystal structure of phytoferritin. To elucidate the function of the transit site in ferritin from other species, we prepared transit-site-deficient mutants of human H ferritin, E140A and E140Q, and their iron oxidation kinetics was analyzed. The initial velocities of iron oxidization were reduced in the variants, especially in E140Q. The crystal structure of E140Q showed that the side chain of the mutated Gln140 was fixed by a hydrogen bond, whereas that of native Glu140 was flexible. These results suggest that the conserved transit site also has a function to assist with the metal ion sequestration to the ferroxidase site in ferritins from vertebrates.

1. Introduction

Ferritin is a ubiquitous iron storage protein that possesses ferroxidase activity (E.C. 1.16.3.1). In general, ferritin molecules form hollow, spherical cage-shaped oligomers composed of 24 subunits, which can be related by two, three and fourfold symmetry axes. The outer diameter of the oligomer is approximately 120 Å while the diameter of the inner cavity is around 80 Å. Thousands of iron molecules can be incorporated into the inner cavity via ferroxidation occurring in the ferroxidase site [1,2]. In vertebrates, ferritin usually functions as a hetero-polymer composed of two distinct subunits, the H (Heavy) chain and the L (Light) chain. The H and L chain composition of ferritins is tissue specific, e.g., L-chain-rich ferritin is found in the tissues involved in long-term storage of iron such as the liver, while H-chain-rich ferritin is found in the tissues with more active iron metabolism such as muscle. The H chain possesses the ferroxidase site and mainly contributes to the oxidative incorporation of iron, whereas the L chain lacks the ferroxidase site [1,2]. Two major active sites have been identified as the key sites for the iron incorporation: (1) the hydrophilic channel around the threefold symmetry axes; and (2) the ferroxidase site. Iron, usually ferrous iron, enters from the hydrophilic threefold channel (iron entry) [3] and is then transferred to the ferroxidase site and oxidized (ferroxidation), then is sequestered to the side chains of acidic amino acid residues positioned on the inner cavity surface (nucleation). The threefold channel forms a funnel-like structure lined with the acidic residues Asp131 and Glu134 in the human H chain. In the known crystal structures, one to three metal ions are seen in this channel. After entry from the channel, iron atoms are sequestered to the ferroxidase site, which is composed of six amino acid residues, namely Glu27, Tyr34, Glu62, His65, Glu107 and Gln141, in the human H chain [4]. Ferrous irons are oxidized and generate a μ-1,2-peroxodiFe(III) intermediate, which immediately decays to a μ-oxo(hydroxo)-bridged diFe(III) intermediate [5–8].

Although active sites in the iron storage process have been discovered and well characterized, the connections between the known active sites have not been clarified in detail. Recently, Turanoa and co-workers suggested that the ferrous iron was translocated in the 4-helix bundle from the ferroxidase site to the E-helix positioned around the fourfold symmetry axes [9]. Concerning the translocation from the entry channel to the ferroxidase site, we identified a novel metal-binding site, known as the 'transit site', in the crystal structure of soybean ferritin no. 4 (SFER4) [10]. The metal ion at the transit site is coordinated by the side chain of Glu173 and the carbonyl oxygen of the main chain of Thr168. These residues, especially Glu173 of SFER4, are strictly conserved in ferritins from other species. Glu173 corresponds to Glu140 of the human H and L chains. Almost all of the reported sequences of vertebrate ferritin have this glutamate residue; however, in an exception, this residue is substituted for by lysine in the sequence of the mouse L chain. Santambrogio et al. suggested that this substitution causes the low iron incorporation activity of the mouse L chain compared with the human L chain [11].

* Corresponding author. Fax: +81 774 38 3761.
E-mail address: masutaro@kais.kyoto-u.ac.jp (T. Masuda).

0006-291X/$ - see front matter © 2010 Elsevier Inc. All rights reserved.
doi:10.1016/j.bbrc.2010.08.017

Here, to confirm the function of the transit site in vertebrate ferritin, we have compared the ferroxidase activity of the human H chain with its variants, E140A and E140Q, whose transit sites were substituted for by alanine and glutamine, respectively. According to the fast kinetics assay, the mutants showed a delay in ferroxidase activity, especially in the E140Q mutant. These results were supported by the X-ray crystallographic analysis of these molecules. Thus, the transit site was proven to assist with the metal ion movement in vertebrate ferritin as well as phytoferritin.

2. Materials and methods

2.1. Protein expression and purification

Construction of the expression plasmid for human H ferritin was performed in a way similar to that described previously [12]. In brief, the cDNA of the human H ferritin (Accession no. BC016009) encoding 182 amino acids were amplified by PCR using the primer set of (5′-ACGACCGCGTCCACCTCGCAG-3′) and (5′-GCGAAGGATCCTTAGCTTTCATTATCACTG-3′). The resulting fragment was 5′-phosphorylated and digested by *Bam*HI. The sticky end of the product of *Nco*I digestion of pET21d (Novagen) was blunted by T4 DNA polymerase (Takara) then digested by *Bam*HI. The resultant human H fragment and pET24d digest were ligated to construct an expression plasmid of pET_humanH. The expression plasmids for the variants E140A and E140Q were obtained by oligonucleotide site-directed mutagenesis using pET_humanH as a template. These expression plasmids were introduced into the *Escherichia coli* strain BL21(DE3) (Novagen). The positive transformants of each construct were grown at 37 °C on LB medium supplemented with 50 mg/l of carbenicillin. Protein expression was induced with 100 μM IPTG (isopropyl β-D-1-thiogalactopyranoside) when the cell density reached an A_{600} of 0.6. Eventually, the cells were harvested by centrifugation after 3 h of induction and resuspended in buffer A (10 mM Tris–HCl pH 7.5, 1 mM EDTA (ethylenediaminetetraacetic acid), 0.15 M NaCl, 0.1 mM *p*-APMSF (*p*-amidinophenyl methanesulfonyl fluoride hydrochloride), 0.2 μM pepstatin, 0.5 g/l leupeptin) to the concentration of 40 g (fresh weight bacteria)/L, followed by disruption by sonication. The supernatant of the resulting crude extract was collected by centrifugation and incubated at 60 °C for 10 min. The heat stable supernatants were further purified by ammonium sulfate fractionation (40–60% saturated fraction), anion exchange chromatography and size exclusion chromatography according to the purification method for soybean ferritin described previously [10].

2.2. Kinetics assay of iron core formation

Apo-ferritins were prepared using thioglycolic acid as a reductant as described previously [13]. The prepared apo-ferritin was dialyzed against the working buffer (50 mM HEPES-Na, pH 7.0). Concentrations of purified proteins were adjusted to 2.0 μM by the absorbance at 280 nm [14]. Single wavelength stopped-flow kinetics experiments were performed using the SX.18MV stopped-flow instrument (Applied Photophysics). Equal 50 μl volumes of a weakly acidic $(NH_4)_2Fe(SO_4)_2$ solution (24–96 μM) and a buffered apo-ferritin solution (2 μM) were mixed at 25 °C in the thermostatted sample compartment containing a 20 μl quartz stopped-flow cuvette with a 0.2 cm path length. All quoted concentrations are the final concentrations obtained after mixing the two reagents together. Fe(II) oxidation was monitored by the absorbance at 310 nm, which is the specific absorption maximum of μ-oxo-bridged Fe(III) species [6]. Data were acquired every 12.5 ms. The molar absorptivity of 4570 ($cm^{-1}M^{-1}$), which was calculated for μ-oxo-bridged Fe(III) [6], was used to calculate the kinetic parameters. The initial rates were determined by a linear fit of the data points from 0 to 50 ms after mixing, representing the first phase of the iron oxidation kinetics curve. The initial velocities were measured from four to five independent experiments at each Fe concentration.

2.3. Crystallization, data collection and structure determination

Purified human H ferritin and its variants were concentrated to 10 mg/ml in a buffer consisting of 10 mM Tris–HCl at pH 7.5 and 0.15 M sodium chloride. Crystals of native human H ferritin were

Table 1
Data collection and refinement statistics for the crystals of human H ferritin and its variants, E140A and E140Q.

	Native	E140A	E140Q
Data collection statistics			
Beam line	BL26B1	BL38B1	BL38B1
Space group	F432	F432	F432
Lattice parameter (Å)	182.723	182.974	182.354
Wave length (Å)	0.9	0.9	0.9
Resolution (highest shell) (Å)	20–1.52 (1.57–1.52)	50–1.9(1.97–1.9)	50–1.58 (1.64–1.58)
No. of unique reflections	40.578	21.170	36.077
Completeness (%)	99.9 (98.6)	99.7 (100)	99.9 (100)
Data redundancy	30.6 (10.9)	15.3 (13.9)	20.1 (18.3)
Rmerge	0.049 (0.352)	0.073 (0.325)	0.046 (0.383)
$I/\sigma(I)$	9.6 (2.71)	19.5 (12.7)	20.5 (11.2)
Refinement statistics			
Protein molecules per asymmetric unit		1	
No. of atoms			
Protein	1473	1476	1464
Solvent	229	192	200
Mg^{2+}	12	10	11
R_{work}/R_{free}	0.171/0.183	0.178/0.218	0.175/0.185
Rms deviations from ideality			
Bond length (Å)	0.006	0.006	0.006
Bond angle (°)	0.966	0.967	0.955
Average B-factor ($Å^2$)			
Main chain	10.1	16.5	14.0
Side chain	14.1	20.4	18.2
Water	22.0	25.7	26.1
Mg^{2+}	20.0	19.5	26.3
Rms deviations from native	–	0.403	0.523

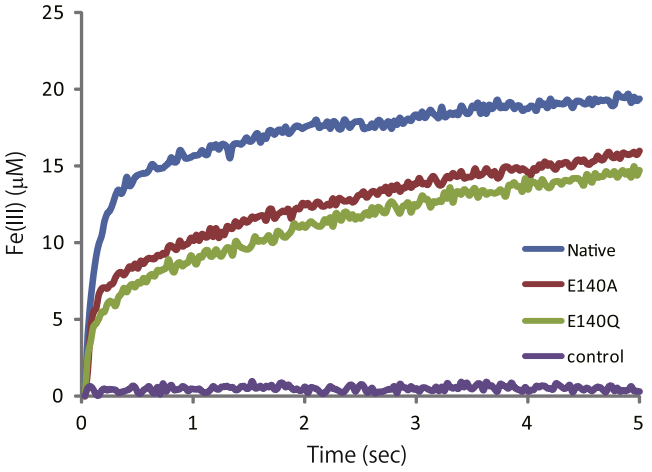

Fig. 1. Ferrous oxidation by ferroxidase sites of native human H ferritin and its variants, E140A and E140Q. Progress curves for the generation of ferric oxo species monitored at 310 nm were plotted every 25 ms, after rapid mixing of solutions of ferrous iron sulfate ammonium (96 μM in 0.1 mM HCl) and recombinant ferritin proteins (2 μM of 24-mer in 50 mM HEPES-Na, pH 7.0). The progress curve of the sample without any apo-ferritin was also plotted as a control. The formation of μ-oxo-bridged Fe(III) was calculated from the absorbance at 310 nm using the molar absorptivity. Data are given as the means of at least four individual experiments.

obtained using the hanging drop vapor diffusion method by mixing equal volumes of the protein sample and mother liquid, which was composed of 0.1 M BICINE-Na at pH 9.0 and 1.9–2.0 M of magnesium chloride. Cubic crystals (space group F432; $a = b = c = 182.5$ Å; $V_M = 2.99$ Å^3/Da for one subunit per asymmetric unit) appeared within a week at 20 °C. The crystallization conditions for the variants, E140A and E140Q, were the same as that of the native crystal. Diffraction data of the crystals of the native, E140A and E140Q variants were collected to resolutions of 1.52, 1.9 and 1.58 Å at 100 K at the SPring-8 beamline BL38B1 and BL26B1 after flash cooling with 30% glycerol as a cryoprotectant. Data were processed, merged and scaled with the HKL-2000 (HKL Research) [15]. Data processing statistics are shown in Table 1.

The structure of native human H ferritin was determined using the deposited structure of the human H chain (PDB ID: 2FHA) and the current data set. Refinement was performed using the REFMAC5 program [16] and PHENIX software [17]. The structure was rebuilt using COOT 0.6.1 [18] on a σ-weighted ($2|F_o|-|F_c|$) and ($|F_o|-|F_c|$) electron density map. The structures of the variants, E140A and E140Q, were determined using the final model of the native human H ferritin, and the refinement strategy was the same as that used for the native. Final refinement statistics for these proteins are shown in Table 1. Figs. 2 and 3 were produced by PyMOL (DeLano Scientific, San Carlos, CA). Structure factors and coordinates have been deposited in the RCSB Protein Data Bank with accession codes, 3AJO (native human H chain), 3AJP (E140A) and 3AJQ (E140Q).

3. Results

3.1. Initial velocity of iron oxidation in native H ferritin and its variants

To evaluate the function of the transit site in iron sequestration to the ferroxidase site in human H chain ferritin, we prepared purified native H ferritin and its transit site variants, E140A and E140Q, and analyzed their iron oxidation/nucleation activity. The proper oligomeric formation of the variants was verified by gel filtration (data not shown). UV spectral absorption at 305–330 nm has been traditionally used to monitor the ferroxidase activity of ferritins. The absorbance around the wavelength, which is characteristic of μ-oxo-bridged Fe(III) dimmers, increases as a result of the Fe(II) oxidation in the ferroxidase site of ferritin. Fig. 1 shows the time-dependent increase of the absorbance at 310 nm in a rapid kinetics assay of ferritin species in which 96 μM of Fe(II) was mixed with 2 μM of ferritin (1/1 Fe(II) atoms per ferroxidase site). The initial velocity of native human H ferritin was 63.1 ± 7.17 μM/s, whereas those of the variants E140A and E140Q were 36.2 ± 4.47 and 29.0 ± 1.56 μM/s, respectively. All the calculated values were significantly different ($P < 0.01$) in the variants. Furthermore, the values were also significantly different between two variants ($P < 0.05$). These tendencies were also observed at the ferritin/Fe(II) ratios of 2/48 (data not shown). These results showed a delay in iron oxidation and core formation in the transit site variants of human H ferritin, among which the rate in the E140Q variant was rather strongly affected.

3.2. Three-dimensional structural analysis of native human H ferritin and its variants

To investigate why the rates of iron oxidation and core formation were affected differently in the variants, we crystallized the native human H ferritin and its variants and performed structural analyses. Until now, crystallizations of the human H chain were performed using the mutant K86Q, in which the surface lysine residue is substituted for glutamine [4,19]. However, we obtained highly symmetrical cubic crystals (space group F432) of human H ferritin without any modifications. Crystals of the transit site variants, E140A and E140Q, were obtained in a condition similar to native crystallization. In these crystals, inter-molecule contact was mediated by magnesium ions positioned around the side chains of Asp84 and Lys86 (Fig. 2A). The statistics regarding the data collection for and refinement of these crystals are shown in Table 1. Diffraction data sets of native human H, E140A and E140Q were collected up to resolution of 1.52, 1.9 and 1.58 Å, respectively. The final structural models of the native and its variants showed good geometries. The root mean square distances of all atoms of the proteins were 0.403 (between native and E140A) and 0.523 (between native and E140Q) (Table 1), suggesting that the structures are nearly identical except for the mutated residues. At the ferroxidase sites, a magnesium ion was seen in conventional site A, which was coordinated by Glu27, Glu62 and His65, while site B of the native and its variants were not occupied in this crystallization condition (Fig. 2B). Instead of the conventional site B, a magnesium ion is seen adjacent to the ferroxidase site, and this ion is coordinated by the side chains of the ferroxidase member, Glu61, and Gln58 (Fig. 2B). We define this site as 'site B′' in this article. Site B′ is more accessible from the inner cavity and the transit site, Glu140. The geometries of the amino acid residues, water molecules and coordinated magnesium ions around the ferroxidase sites of all ferritins are nearly identical, suggesting that the ferroxidase sites of the variants were not disrupted by the transit site mutation. Other magnesium ions are seen around the threefold symmetry channel (Asp131 and Glu134), fourfold symmetry channel (His173), outer surface (Asp84 and Lys86) and near the transit site (Glu140). Among these binding sites, three magnesium ions are seen around the funnel-like threefold symmetry channel (Fig. 2C and D) in accordance with previous studies [19]. The first magnesium ion from the entrance of the channel is coordinated by the side chain of Glu134, the second is coordinated by the side chains of Glu134 and Asp131, and the third, which also faces the inner cavity, is coordinated by the side chain of Asp131. The first and second magnesium ions appear on the threefold symmetry axes (Fig. 2C).

The transit site of the native H ferritin, Glu140, was disordered and had two or more alternative conformations (Fig. 3A), whereas the conformation of the side chains of the transit sites in the vari-

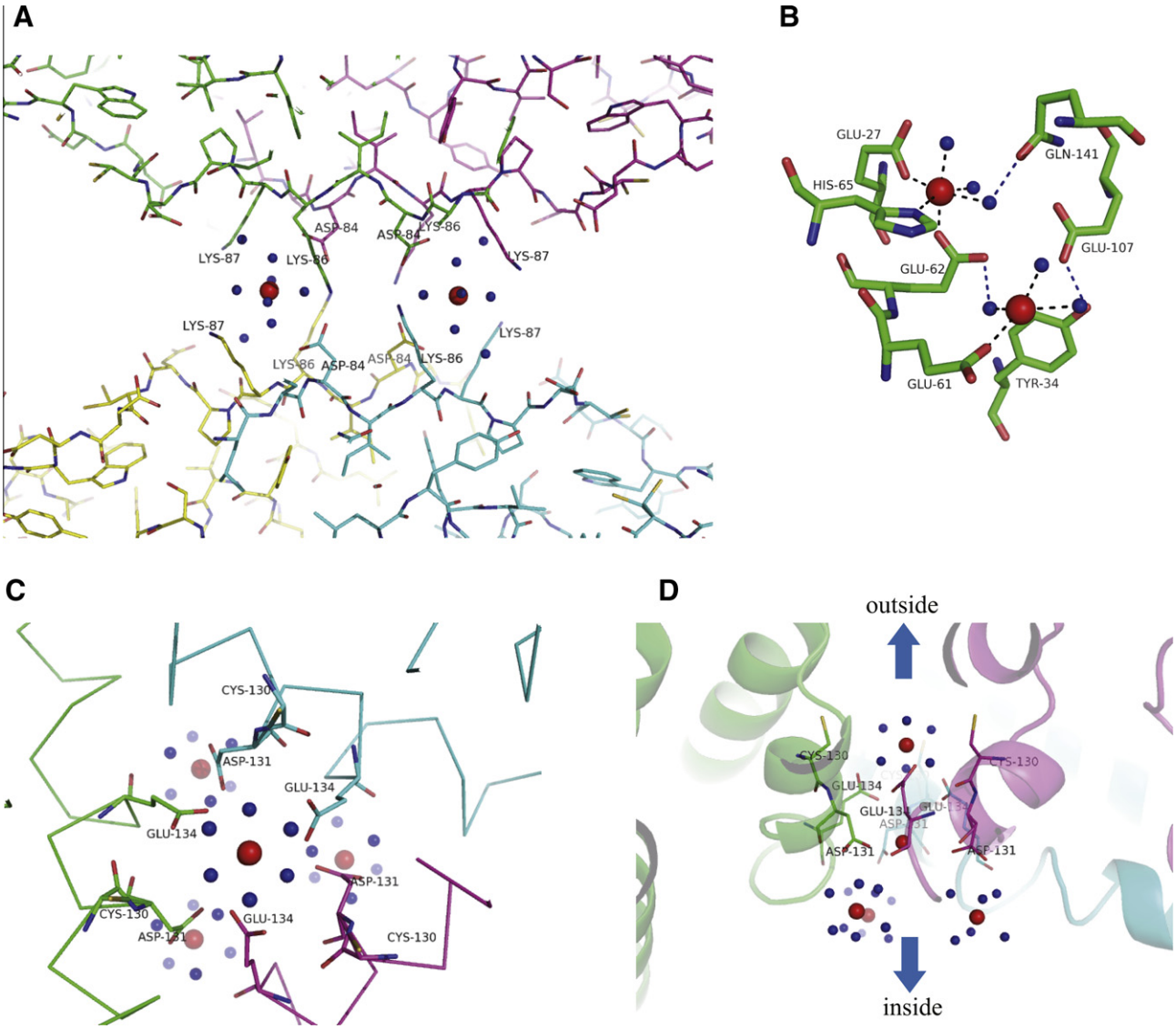

Fig. 2. (A) Inter-molecule contact of the crystal structure of native human H ferritin. Involved subunits are shown in green, purple, cyan and yellow chains. The magnesium ions and water molecules are shown as red and blue balls. (B) Ferroxidase site of native human H ferritin. Metal-coordinated bonds and hydrogen bonds are shown in black and blue broken lines, respectively. (C, D) The structure of the metal ion entry channel penetrating along the threefold symmetry axis and metal-binding site in the channel. The channels are represented with two different orientations: (C) aligned on the threefold axis and (D) perpendicular to the axis.

ants were unambiguously determined in their crystal structures (Fig. 3B and C). In one of the alternative conformations of Glu140, the side chain is oriented toward the threefold entry channel, while in another conformation it is oriented toward site B′ of the ferroxidase site. In E140A, the substitution of the transit site to alanine caused a hydrophilic route to develop from the threefold symmetry axes to the ferroxidase site, as in the case of the soybean ferritin E173A variant [10]. On the other hand, the substituted glutamine side chain was hydrogen-bonded to a water molecule, which was not seen in the crystal structure of the native and E140A (Fig. 3C). In addition to the hydrogen bond with the Gln140 side chain (2.56 Å), this water molecule formed hydrogen bonds with the main chain oxygen of Glu134 and Thr135 (2.63 and 3.04 Å, respectively), and the main chain nitrogen of Asn139 (2.83 Å), resulting in the fixation of the glutamine side chain (Fig. 3D). This side chain fixation caused the blockage of the hydrophilic route, which enabled the passage of metal ions or water molecules.

4. Discussion

Recently, the pathway for metal ion movement in the ferritin shell has received a great deal of research attention. As the active sites for iron sequestration in ferritin, two major components have been identified, namely the acidic residues lining the threefold channel and the ferroxidase site. These sites have been identified as active sites for the metal sequestration process of ferritin. It has been suggested that the channels around the threefold symmetry axes mainly function as iron entry channels for ferritin [3]. In this study, we have identified three magnesium ions in the channel (Fig. 2C and D). These arrangement of magnesium ions are reminiscent the metal ion pathway from the outer part of the shell to the inner cavity through the channel, because this channel is the only entrance for the metal ions [20]. In contrast to the observation by Toussaint et al., Cys130, which was positioned at the entrance to the threefold channel, did not have alternative conformations, and no metal ion was seen to be coordinated with this residue in

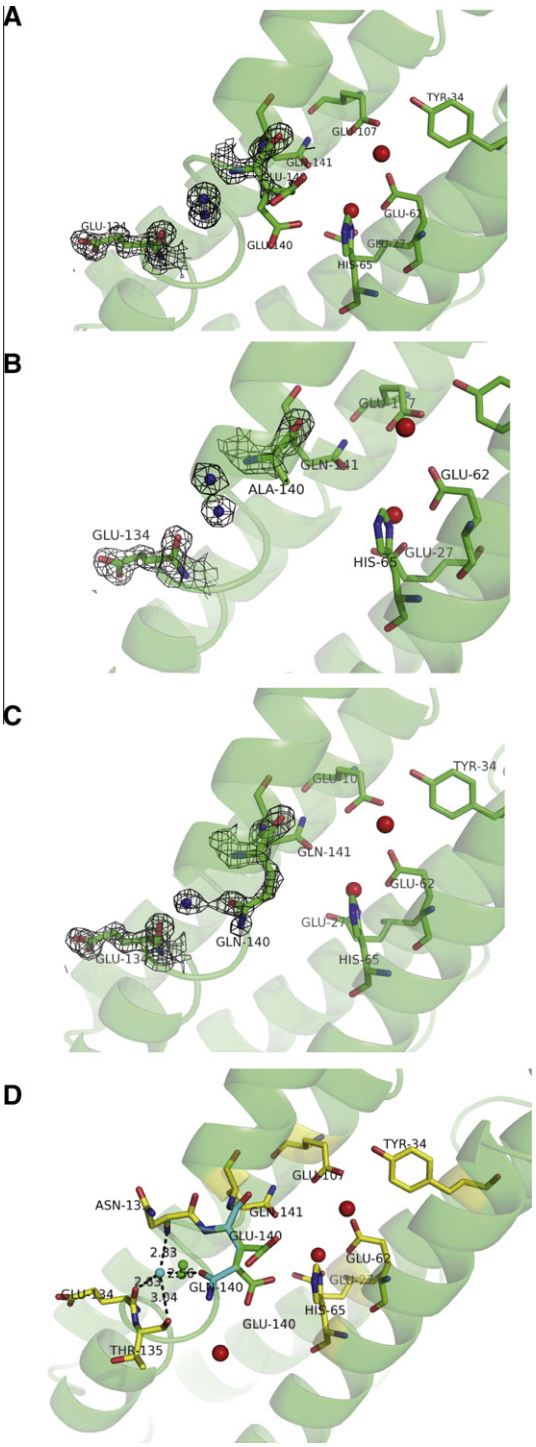

Fig. 3. Structures around the transit site in the native H chain (A) and its variants, E140A (B) and E140Q (C). The electron densities ($2|F_o| - |F_c|$) contoured 2.0 σ of the transit sites and Glu134 together with the hydrogen-bonded water molecules are shown as mesh. Ferroxidase sites and binding magnesium ions are also represented. The magnesium ions and water molecules are shown as red and blue balls. (D) Comparison of the structures around the transit sites of the native H ferritin and the E140Q variant. The side chains of Glu140 alternative conformations in the native H chain are shown in green, while the side chain of Gln140 is shown in cyan. The magnesium ions are shown as red balls. Water molecules shown in the coordinates of the native structure or E140Q variant are shown as green and cyan balls. The distances of the hydrogen bonds between the water molecule in E140Q and the adjacent atoms are shown (Å).

our crystal structure [19]. The alternative conformation of the side chain of this cysteine is suggested to facilitate metal ion entry into the channel [19]. Even though there was no such tendency in the cysteine residue in our crystal structure, this cysteine residue may be part of a pathway of metal ion movement in vertebrate ferritin, because it has also been reported that the cysteine residue (Cys126 of the L chain ferritin) binds a metal (Pd) ion, and it has been suggested that this residue forms a pathway for metal ion movement [21]. This cysteine residue may constitute the first contact for metal ions at least in vertebrate ferritin, after which the metal ions are transferred to Glu134 and/or Asp131. However, this cystein residue is absent in plant or bacterial ferritin. Concerning the translocation of metal ions among the active sites, it was suggested that the Glu61 assists with the metal ion movement from the ferroxidase site to the inner cavity, mainly because the residue in the crystal structure has two alternative conformations [4]. More recently, Turano et al. demonstrated that the iron(III) species oxidized in the ferroxidase site was translocated in the 4-helix bundle to the E-helix positioned around the fourfold symmetry axes using NMR spectrometry [9]. In contrast, there have been few studies that have described the metal ion movement from the threefold symmetry channel to the ferroxidase site. In relation to this movement, we have identified a transit site in the crystal structure of soybean ferritin [10]. This site, Glu173 of the soybean ferritin (SFER4), is a highly conserved residue among ferritins from various species. In this study, we have demonstrated that Glu140 of the human ferritin H chain, corresponding to Glu173 of SFER4, also functions as a transit site in human H chain ferritin. The transit site variants, E140A and E140Q, have shown a delay in the iron oxidation/nucleation rate compared with that of native human H similar to the case of the rapid kinetics assay of soybean ferritin and its transit site variants (Data not shown). Furthermore, the iron oxidation/nucleation rate of E140Q was found to be slower than that of E140A. In the E140A variant, a new hydrophilic route emerged from the threefold symmetry axes to the ferroxidase site, much like the case of soybean ferritin [10]. These hydrophilic routes enable the metal ions to pass through. On the other hand, the side chain of the substituted Gln140 was fixed by the hydrogen bond formed with a water molecule, which was hydrogen-bonded to the main chain oxygen of Glu134. This side chain fixation may hinder the ions from following the route toward the ferroxidase site. The side chain of the Glu140 of native human H ferritin did not form any hydrogen bonds; therefore, it can move freely to assist in the metal ion movement from the threefold channel to the ferroxidase site. These results support the hypothesis that the glutamate residue, Glu140, in the human H chain also acts as the transit site as seen in soybean ferritin.

Thus, we have demonstrated the significance of the transit site in iron loading to the ferroxidase site. Together with the metal-binding sites in the threefold channel, we can postulate that the pathway for metal ion movement from outside of the threefold channel to the ferroxidase site via the transit site in ferritins is as follows. Metal ions are incorporated into the threefold channel of ferritin with the assistance of the Cys130 side chain in vertebrate ferritin. They are then captured by Glu134 and transfered to Asp131. Next, ferrous ions are guided to the transit site, Glu140, via Thr135 and His136. The side chain of the transit site, Glu140, brings metal ions to site B′ of the ferroxidase site and, ultimately, ferrous ions are oxidized in ferroxidase sites A and B. The transit site is further conserved in ferritins from prokaryotes. Whether the conserved acidic residue functions as the transit site in iron accumulation in prokaryotic ferritins remains a very intriguing question.

Acknowledgments

The synchrotron radiation experiments were performed at BL38B1 and BL26B1 in SPring-8 with the approval of the Japan Syn-

chrotron Radiation Research Institute (JASRI) (proposal number 2010A1234). This work was supported by Grants-in-aid for Young Scientists from the Ministry of Education, Culture, Sports, Science and Technology of Japan (22780303), and a grant from the Shorai Foundation for Science and Technology.

References

[1] P.M. Harrison, P. Arosio, The ferritins: molecular properties iron storage function and cellular regulation, Biochim. Biophys. Acta 1275 (1996) 161–203.
[2] E.C. Theil, Ferrit structure, gene regulation, and cellular function in animals, plants and microorganisms, Ann. Rev. Biochem. 56 (1987) 289–315.
[3] M.J. Yablonski, E.C. Theil, A possible role for the conserved trimer interface of ferritin in iron incorporation, Biochemistry 31 (1992) 9680–9684.
[4] D.M. Lawson, P.J. Artymiuk, S.J. Yewdall, J.M.A. Smith, J.C. Livingstone, A. Treffry, A. Luzzago, S. Levi, P. Arosio, G. Cesareni, C.D. Thomas, W.V. Shaw, P.M. Harrison, Solving the structure of human H ferritin by genetically engineering intermolecular crystal contacts, Nature 349 (1991) 541–544.
[5] S. Sun, P. Arosio, S. Levi, N.D. Chasteen, Ferroxidase kinetics of human liver recombinant apoferritin H-chain apoferritin and site-directed mutants, Biochemistry 32 (1993) 9362–9369.
[6] X. Yang, Y. Chen-Barrett, P. Arosio, N.D. Chasteen, Reaction paths of iron oxidation and hydrolysis in horse spleen and recombinant human ferritins, Biochemistry 37 (1998) 9743–9750.
[7] G.N. Jameson, W. Jin, C. Krebs, A.S. Perreira, P. Tavares, X. Liu, E.C. Theil, B.H. Huynh, Stoichiometric production of hydrogen peroxide and parallel formation of ferric multimers through decay of the diferric-peroxo complex the first detectable intermediate in ferritin mineralization, Biochemistry 41 (2002) 13435–13443.
[8] X. Liu, E.C. Theil, Ferritin reactions: direct identification of the site for the diferric peroxide reaction intermediate, Proc. Natl. Acad. Sci. USA 101 (2004) 8557–8562.
[9] P. Turanoa, D. Lallia, I.C. Fellia, E.C. Theil, I. Bertini, NMR reveals pathway for ferric mineral precursors to the central cavity of ferritin, Proc. Natl. Acad. Sci. USA 107 (2010) 545–550.
[10] T. Masuda, F. Goto, T. Yoshihara, B. Mikami, Crystal structure of plant ferritin reveals a novel metal binding site that functions as a transit site for metal transfer in ferritin, J. Biol. Chem. 285 (2010) 4049–4059.
[11] P. Santambrogio, A. Cozzi, S. Levi, E. Rovida, F. Magni, A. Albertini, P. Arosio, Functional and immunological analysis of recombinant mouse H- and L-ferritins from *Escherichia coli*, Protein Expression Purif. 19 (2000) 212–218.
[12] T. Masuda, F. Goto, T. Yoshihara, T. Ezure, T. Suzuki, S. Kobayashi, M. Shikata, S. Utsumi, Construction of homo- and heteropolymers of plant ferritin subunits using an in vitro protein expression system, Protein Expression Purif. 56 (2007) 237–246.
[13] N.D. Chasteen, E.C. Theil, Iron binding by horse spleen apoferritin. a vanadyl(IV) EPR spin probe study, J. Biol. Chem. 257 (1982) 7672–7677.
[14] C.N. Pace, F. Vajdos, L. Fee, G. Grimsley, T. Gray, How to measure and predict the molar absorption coefficient of a protein, Protein Sci. 4 (1995) 2411–2423.
[15] Z. Otwinowski, W. Minor, Processing of X-ray crystallographic data collected in oscillation mode, Methods Enzymol. 276 (1997) 307–326.
[16] G.N. Murshudov, A.A. Vagin, E.J. Dodson, Refinement of macromolecular structures by the maximum-likelihood method, Acta Crystallogr., Sect. D: Biol. Crystallogr. 53 (1997) 240–255.
[17] P.D. Adams, R.W. Grosse-Kunstleve, L.W. Hung, T.R. Ioerger, A.J. McCoy, N.W. Moriarty, R.J. Read, J.C. Sacchettini, N.K. Sauter, T.C. Terwilliger, PHENIX: building new software for automated crystallographic structure determination, Acta Crystallogr., Sect. D: Biol. Crystallogr. 58 (2002) 1948–1954.
[18] P. Emsley, K. Cowtan, Coot: model-building tools for molecular graphics, Acta Crystallogr., Sect. D: Biol. Crystallogr. 60 (2004) 2126–2132.
[19] L. Toussaint, L. Bertrand, L. Hue, R.R. Crichton, J.P. Declercq, High-resolution X-ray structures of human apoferritin H-chain mutants correlated with their activity and metal-binding sites, J. Mol. Biol. 365 (2007) 440–452.
[20] F. Bou-Abdallah, G. Zhao, G. Biasiotto, M. Poli, P. Arosio, N.D. Chasteen, Facilitated diffusion of iron(II) and dioxygen substrates into human H-chain ferritin. A fluorescence and absorbance study employing the ferroxidase center substitution Y34W, J. Am. Chem. Soc. 130 (2008) 17801–17811.
[21] T. Ueno, M. Abe, K. Hirata, S. Abe, M. Suzuki, N. Shimizu, M. Yamamoto, M. Takata, Y. Watanabe, Process of accumulation of metal ions on the interior surface of apo-ferritin: crystal structures of a series of apo-ferritins containing variable quantities of Pd(II) ions, J. Am. Chem. Soc. 131 (2009) 5094–5100.